water

MDPI

Article

Numerical Study on the Effect of Crown Clearance Thickness on High-Head Pump Turbines

Lei Li [1], Dandan Yan [2], Xuyang Liu [1], Weiqiang Zhao [3], Yupeng Wang [1], Jiayang Pang [2] and Zhengwei Wang [3,*]

[1] Henan Luoning Pump-Storage Power Co., Ltd., Luoyang 471721, China; lilei@luoningpsps.com (L.L.); lncxlxy@126.com (X.L.); m13772112350@163.com (Y.W.)
[2] College of Water Resources and Civil Engineering, China Agricultural University, Beijing 100083, China; yan1550319145@163.com (D.Y.); pangjy9603@163.com (J.P.)
[3] State Key Laboratory of Hydroscience and Engineering, Department of Energy and Power Engineering, Tsinghua University, Beijing 100084, China; zhaoweiqiang@mail.tsinghua.edu.cn
* Correspondence: wzw@mail.tsinghua.eud.cn; Tel.: +86-13601363209

Abstract: In order to promote the development of new power systems and the consumption of clean energy, pumped storage hydropower stations tend to become increasingly larger in capacity and higher in head height. In this paper, a three-dimensional model of the full channel of a high-head pump turbine is established, and the influence of the gap thickness between the runner crown and the headcover on the internal flow field characteristics, pressure fluctuation characteristics and axial water thrust are studied by means of computational fluid dynamics (CFD). The results indicate that the area where the pressure and velocity vary greatly in the flow field of the crown clearance is at the seal of the labyrinth ring. In addition, the pressure balance pipe has a greater impact on the pressure and flow rate of the water passing through the clearance, and the crown clearance near the pressure balance pipe generates a vortex, resulting in energy loss. Decreasing the thickness of the clearance has no obvious effect on the pressure on the flow-passing components, and increasing the thickness of the clearance has a great change in the pressure values at the upper crown inlet, in front of the labyrinth ring of the crown and in front of the labyrinth ring of the band. The upper part of the vaneless area, the crown inlet and the lower ring inlet are close to the runner; hence, the interference from the rotating parts is the strongest. The effect of increasing the thickness of the crown clearance on the axial water thrust is greater than that of decreasing the thickness of the crown clearance. The pulsation frequency of the axial thrust on the crown, band and blade and the resultant force of the axial thrust increase with the increase in the crown clearance thickness.

Keywords: flow characteristics; axial force; clearance; CFD; pump turbine

Citation: Li, L.; Yan, D.; Liu, X.; Zhao, W.; Wang, Y.; Pang, J.; Wang, Z. Numerical Study on the Effect of Crown Clearance Thickness on High-Head Pump Turbines. *Water* **2023**, *15*, 3397. https://doi.org/10.3390/w15193397

Academic Editor: Helena M. Ramos

Received: 7 August 2023
Revised: 12 September 2023
Accepted: 18 September 2023
Published: 27 September 2023

1. Introduction

Pumped Storage Hydropower (PSH) is currently one of the most mature energy storage technologies in the world [1] and the largest to date [2]. PSH has flexibility and good storage capacity, so it has been widely used in the field of renewable energy power generation [3,4]. At present, China is in a critical period of green and low-carbon energy transformation and development. With the large-scale and high-proportion development of new energy sources such as wind power and photovoltaic power generation, the demand for power regulation is more urgent. The construction of a new power system with new energy as the main body puts forward higher requirements for the development of pumped storage [5]. In a pumped storage unit, because the high-head pump turbine has many advantages, such as a high speed, small flow, small size and high head, the design of the pump turbine has recently tended to have a high head [6]. Due to the higher pressure of the high head unit, the gap leakage problem is more obvious than that of the ordinary unit, which is a scientific problem that needs to be solved urgently.

Clearances cause leakage losses due to part of the water not flowing through the runner and friction losses due to torque applied to the rotor [7]. Kim SJ et al. [8] studied the gap flow characteristics of the upper and lower rings of the Francis turbine runner and compared the changes in the hydraulic performance and flow characteristics of the unit with and without gaps.

The magnitude of the axial water thrust on the runner gap can often affect the stability of the unit in the axial direction, so the change in the axial water thrust caused by the gap has been deeply studied by several scholars. Studies have shown that, under load shedding conditions, the gap flow between the runner and the fixed part determines the precise simulation of the pump turbine pulsation characteristics and unsteady vortex [9]. Hou XX et al. [10] used the method of combining PIV measurements and a numerical simulation to determine the reasons that affect the gap flow pattern and axial water thrust, and they quantitatively expressed the axial water thrust as a function of the square of the rotational speed and the gap inlet pressure. Liu YS et al. [11] studied the influence of different runner sinking axial deviation values on the axial water thrust of Francis turbines under rated conditions and found that, when the runner sinks, the axial water thrust on the upper ring increases, whereas the axial water thrust on the lower ring decreases. Zhou L et al. [12] compared different impeller hub radii on the influence of the axial force, and it was found that the bevel trimming of the hub radius can effectively reduce the axial force.

The axial and radial clearance between the runner and its surrounding components is one of the key factors affecting the performance of the unit according to He LY et al. [13]. The acoustic–solid coupling method and the improved one-way fluid–solid coupling method are used to study the influence of the radial and axial gaps between the runner and the surrounding structure on the additional mass and dynamic stress of the turbine runner. The results show that the axial gap has a greater impact on the additional quality factor of the in-phase, and the radial gap has a greater impact on the additional quality factor of the counter-phase and crown-dominant modes. Wang ZJ et al. [14] studied pressure pulsation in the gap between the runner and the guide vanes through a numerical simulation, and they found that, in this gap, the run-away point in the braking zone of the turbine generates a low-frequency component caused by the rotating stall. When the pump rotates in the reverse direction as a water turbine to generate electricity, the radial clearance between the impeller blade tip and the volute tongue affects the pump as one of the main factors of the turbine's performance. Yang SS et al. [15] calculated the unsteady flow field of a pump as turbine and found that, due to the rotor–stator interaction (RSI) between the impeller and the volute, low-frequency pressure pulsations are generated in the impeller, and high-frequency pressure pulsations are generated in the volute and propagate in the flow channel. When the radial clearance increases, the pressure pulsation amplitude of the impeller remains unchanged, whereas the pressure pulsation amplitude in the volute increases. The authors of [16] compared the numerical results of the gap flow field between the impeller and the pump cover (cover) with the experimental results and found that the two results were very similar, and as the gap increased, the interference of the water flow out of the gap on the impeller inlet flow increased. Yonezawa K et al. [17] used numerical simulation methods to explore the principle of sand erosion in the runner gap and used experimental research methods to study the vortex flow characteristics in the gap. It was found that the second-stage sealing gap inlet was severely eroded, and vortex flow was generated between the first-stage and second-stage sealing gaps. Sonawat A et al. [18] determined the range of the axial clearance and radial clearance that can affect the performance of positive displacement turbines through experimental research.

The mutual interference between the radial gaps of the dynamic and static cascades also has a certain impact on the performance of the turbine. Sato K et al. [19] proposed an unsteady three-dimensional incompressible Navier–Stokes method and carried out a comparative verification of calculations and experiments on a centrifugal pump with a vane diffuser, and they then carried out numerical simulation research on the radial clearance on a hydraulic turbine. The research shows that, as the radial clearance of

the blade cascade decreases, the predicted efficiency of the hydraulic turbine decreases. Shu P et al. [20] studied the effect of the axial clearance between the static cascades of marine steam turbines on the flow field and found that, as the axial clearance increases, the blade pressure fluctuation decreases, but the vortex structure at the blade root increases, resulting in a decrease in unit efficiency.

Some scholars extracted the gap channel and calculated the pure gap separately. When the gap is connected with the mainstream basin, the full channel is generally calculated. In this paper, in order to truly and fully reflect the flow state in the gap and accurately set the boundary conditions, a three-dimensional full channel model is established to calculate the whole basin. The influence of the thickness of the runner crown clearance on the pressure pulsation and axial stability of the runner of a reversible pump turbine is studied by means of a full flow passage numerical simulation. In Section 2, the basic theory and simulation setup, including meshing, border condition configuration, etc., are presented. In Section 3, the calculation results, such as the energy characteristics, pressure distribution and axial hydraulic pressure, are obtained and analyzed. Section 4 gives the main conclusions. The results show that the area with large changes in pressure and velocity in the upper crown clearance flow field is the labyrinth ring seal, and the pressure and velocity of the flow through the gap are greatly affected by the pressure and velocity of the flow through the gap. In addition, the vortex is generated near the pressure and velocity of the upper crown gap. The upper part, the upper crown inlet and the lower ring inlet of the vaneless region are the most disturbed by rotating components. The pulsation frequency of the axial water thrust on the upper crown, the lower ring and the blade and the resultant force of the axial water thrust increase with the increase in the clearance thickness of the upper crown.

2. Computational Fluid Dynamics

2.1. Fluid Dynamics Governing Equations

Fluid flow follows the basic laws of physical conservation, and the three major conservation laws correspond to the three governing equations, including mass conservation equations, momentum conservation equations and energy conservation equations.

2.1.1. Mass Conservation Equation

The mass conservation equation can be described as follows: the increase in mass in the fluid micro-element per unit of time is equal to the net mass flowing into the micro-element in the same time interval. The mass conservation equation is shown in Equation (1).

$$\frac{\partial \rho}{\partial t} + \frac{\partial(\rho u)}{\partial x} + \frac{\partial(\rho v)}{\partial y} + \frac{\partial(\rho w)}{\partial z} = 0 \tag{1}$$

Among them, ρ represents the density, t represents the time, and u, v and w are the components of the velocity vector $\vec{u}$ in the x, y and z directions.

2.1.2. Momentum Conservation Equation

The law of conservation of momentum can be described as follows: the rate of change of the momentum of a fluid in a micro-element with respect to time is equal to the sum of various forces acting on the micro-element from the outside, which is Newton's second law. According to this law, momentum conservation equations in x, y and z directions are derived, as shown in Equations (2)–(4).

$$\frac{\partial(\rho u)}{\partial t} + div\left(\rho u \vec{u}\right) = -\frac{\partial p}{\partial x} + \frac{\partial \tau_{xx}}{\partial x} + \frac{\partial \tau_{yx}}{\partial y} + \frac{\partial \tau_{zx}}{\partial z} + F_x \tag{2}$$

$$\frac{\partial(\rho v)}{\partial t} + div\left(\rho v \vec{u}\right) = -\frac{\partial p}{\partial y} + \frac{\partial \tau_{xy}}{\partial x} + \frac{\partial \tau_{yy}}{\partial y} + \frac{\partial \tau_{zy}}{\partial z} + F_y \tag{3}$$

$$\frac{\partial(\rho w)}{\partial t} + div\left(\rho w \vec{u}\right) = -\frac{\partial p}{\partial z} + \frac{\partial \tau_{xz}}{\partial x} + \frac{\partial \tau_{yz}}{\partial y} + \frac{\partial \tau_{zz}}{\partial z} + F_z \tag{4}$$

Among them, p is the pressure on the fluid micro-body, τ_{xx}, τ_{xy}, τ_{xz}, etc., are the components of viscous stress acting on the surface of the micro-body due to molecular viscosity $\vec{\tau}$, F_x, F_y and F_z are the physical forces on the micro-body, and when the physical force is only gravity, the direction is vertically upward ($F_x = 0$, $F_y = 0$, $F_z = -\rho g$).

2.1.3. SST k–ω Model

The SST k–ω model was developed using Menter's SST model, so it is superior to the k–ε model in a wide range of fields. The k–ω model has a wide range of applications and is accurate in near-wall free flow. In order to achieve this purpose, the k–ε model is modified into the k–ω model. The SST k–ω model is similar to the standard k–ω model, but the SST k–ω model has higher accuracy and reliability compared to the standard k–ω model in a wide range of flow fields. The k–ω model has advantages in predicting flow around a wall and swirling flows.

The complete BSL k–ω equation is shown in Equations (5) and (6).'

$$\frac{\partial(\rho k)}{\partial t} + \nabla \cdot \left(\rho \vec{U} k\right) = \nabla \cdot \left(\left(\mu + \frac{\mu_t}{\sigma_k}\right)\nabla k\right) + P_k - \rho\varepsilon \tag{5}$$

$$\frac{\partial(\rho\omega)}{\partial t} = \nabla \cdot \left(\rho \vec{U} \omega\right) = \nabla \cdot \left(\left(\mu + \frac{\mu_t}{\sigma_k}\right)\nabla\omega\right) + \frac{\gamma}{\nu_t}P_k - \beta\rho\omega^2 + 2(1 - F_1)\frac{\rho\sigma_{\omega 2}}{\omega}\nabla k \tag{6}$$

Based on the complete BSL k–ω equation, the turbulence viscosity limit is introduced to give it wider applications:

$$\mu_t = \frac{\rho k}{\omega}\frac{1}{max\left[\frac{1}{\alpha^*}, \frac{SF_2}{a_1\omega}\right]} \tag{7}$$

where F_2 is another mixed equation, as follows:

$$F_2 = \tanh\left(\arg_2^2\right) \tag{8}$$

$$\arg_2 = max\left[2\frac{\sqrt{k}}{0.09\omega d}, \frac{500\mu}{\rho d^2\omega}\right] \tag{9}$$

2.2. Full Runner 3D Model Establishment and Mesh Division

2.2.1. Full Runner 3D Model

In this paper, a prototype pump turbine model is used as an example. The basic parameters of the researched machine are listed in Table 1.

Table 1. Basic parameters of the researched pump turbine unit.

Parameter	Value
Net head	604 m
Rated output	350 MW
Runner diameter	4.12 m
Rate discharge	64.26 m^3/s
Number of blades Z_b	10
Number of guide vanes Z_g	16
Rotation speed	500 rpm

In order to simulate the real situation of the flow in the gap to the furthest extent possible, the calculation domain of the whole flow channel, including the guide vane, runner, gap, draft pipe and spiral casing, was analyzed. The 3D modeling software UG NX 12.0 was used to build up a three-dimensional model of the spiral casing, runner, draft tube, stay vanes, guide vanes, upper crown clearance and lower ring clearance of a pump turbine. The three-dimensional model of the full flow channel is shown in Figure 1.

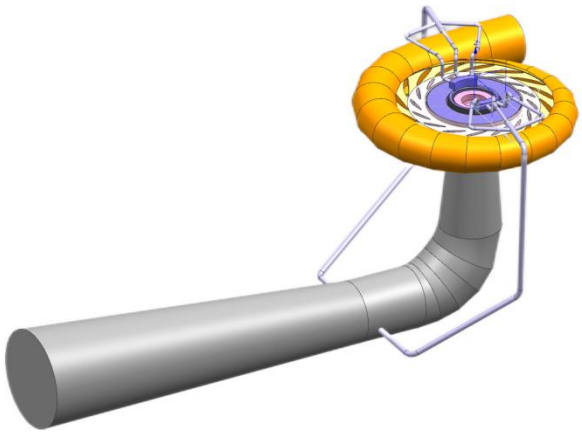

Figure 1. Three-dimensional full channel fluid domain model.

Among them, the thickness of the gap between the upper crown and the top cover of the runner (the upper crown gap) was specifically studied, as shown in Figure 2. The absolute value of the gap thickness is δ, and the dimensionless gap thickness λ is defined as follows:

$$\lambda = \frac{\delta}{D_h} \tag{10}$$

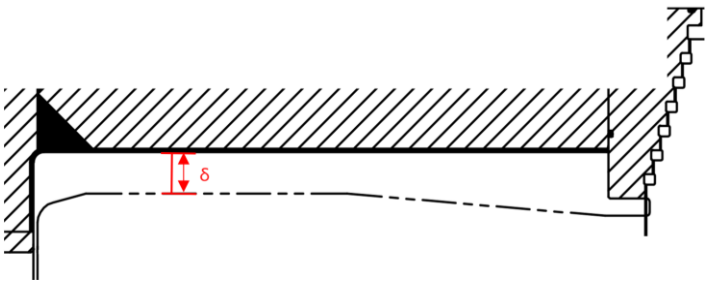

Figure 2. Thickness of the crown gap δ.

In Equation (10), D_h is the runner diameter. In the analysis, the gap thickness coefficient λ increases or decreases by 0.006, 0.011 or 0.023. The changes of the internal flow field and the axial force of the pump turbine are then analyzed.

2.2.2. Meshing

A combination of a structured grid and an unstructured grid is used for the pump turbine unit, and the structured grid is used in the geometrically regular area to save storage space and improve computing addressability. Unstructured grids are used in geometrically irregular areas to improve geometric adaptability, improve grid quality and enhance calculation convergence. Among them, the sealing cavity of the upper crown cavity, the sealing cavity of the lower ring cavity, the stay vanes, the guide vanes and the spiral casing are divided into structured grids. Because the runner has a significant impact on the calculation quality, the edge of the runner blade is divided into structured grids.

The three-dimensional fluid domain model is shown in Figure 3, where the three-dimensional flow field calculation area includes the fluid domain of the double row cascade

(Figure 3a), the lower ring gap fluid domain (Figure 3b), the fluid domain of the spiral casing (Figure 3c), the upper crown gap fluid domain (Figure 3d), the flat pressure tube fluid domain (Figure 3e) and the runner fluid domain (Figure 3e). The final numbers of elements of each component are listed in Table 2.

Figure 3. Mesh division of each part: (**a**) Mesh of the double row cascade; (**b**) Mesh of the lower ring gap; (**c**) Mesh of the spiral casing; (**d**) Mesh of the upper crown gap; (**e**) Mesh of the flat pressure tube; (**f**) Mesh of the runner.

Table 2. Type and number of the elements of each component.

Component	Element Type	Element Number
Spiral casing	Hex	1,587,054
Stay vanes	Hex	88,461
Guide vanes	Hex	332,016
Runner	Hex	7,817,175
Upper and lower labyrinth seals	Hex	896,528
Pressure balance pipelines	Hex	334,900
Draft tube	Mix	281,649
Total number	Mix	11,337,783

2.2.3. Boundary Conditions

Boundary conditions refer to the changing law of the variable setting with coordinates and time on the boundary of the calculation solution domain before numerical calculations. The calculation domain of the whole channel of the pump turbine is shown in Figure 4. The calculation is carried out in ANSYS CFX, the medium is selected as water, and the SST k–ω model is selected as the turbulent flow model. Among the commonly used eddy viscous turbulence models, the SST k–ω model is the most widely used. The SST k–ω model is a combination of the k–ω model and the k–ε model, and it can effectively solve low-Reynolds-number flow in the near wall region and flow separation under an inverse pressure gradient. In addition, it has more advantages in the prediction of turbulence with complex wall boundaries. The inlet adopts the total pressure inlet (7.18 MPa), the outlet adopts the static pressure outlet (1.27 MPa), and the solid wall surface adopts the non-slip wall surface. The interface model between the guide vanes and the runner and the interfaces between the runner and the draft tube adopt the Transient Rotor Stator model. The runner domain uses a rotating frame with 500 rpm, and the other fluid domain uses a static frame. According to previous studies, the time step selection is performed according to the time length of the rotation angle between 1° and 3°. Therefore, the time step in this research is selected as 6.67×10^{-4} s.

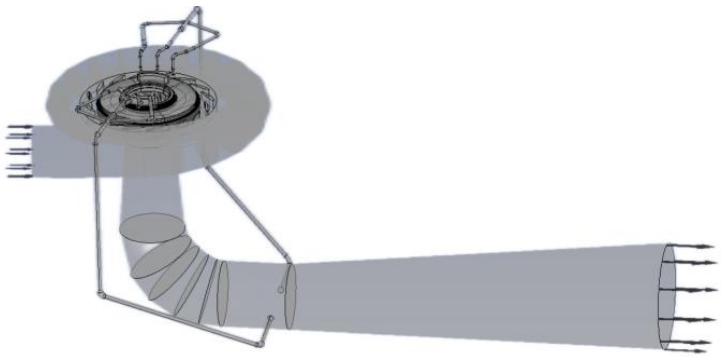

Figure 4. Computational domain of pump turbines.

The high-resolution high-order precision format is selected for the discretization of the convection term and the diffusion term in the calculation process. The time-discrete method of steady calculations is set to a fixed time step, and the convergence accuracy standard is set to 10^{-5}.

3. Calculation Result Analysis

3.1. Mesh Quality Check

Under the working conditions of the turbine, the calculation results of the head, flow rate and power of the unit under rated working conditions are shown in Table 3. The maximum error between the numerical calculation results and the design parameters is 3.94%, which proves the reliability of the numerical calculation method.

Table 3. Comparison between the numerical simulation and the model test.

Item	Head (m)	Flow Rate (m^3/s)	Power (MW)	Efficiency (%)
Numerical calculation	603.43	68.11	371.16	92.37
Design parameters	604	65.71	357.10	92.03
Error (%)	−0.094%	+3.65%	+3.94%	+0.37%

3.2. External Characteristic Analysis

As shown in Figure 5, when setting a reasonable clearance value, its influence on the efficiency η, flow Q, head H, etc., should be considered comprehensively, and the head H is given. As the relative clearance increases, it has little effect on efficiency and flow at first, and it then gradually increases. Increasing the relative gap causes the flow rate to decrease because the leakage of the unit increases with the increase in the gap. In addition, volume loss increases, and the efficiency decreases.

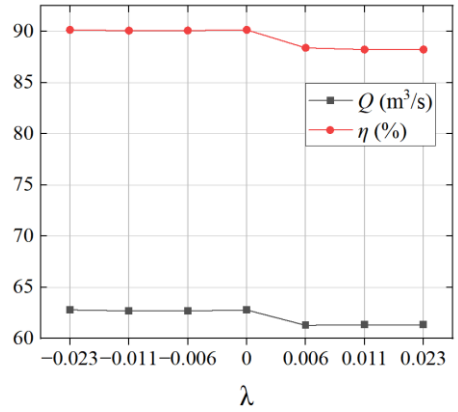

Figure 5. Relationship curves of different gap values and efficiency, flow and head.

3.3. Leakage When the Relative Clearance Is Different

A reasonable runner clearance can reduce clearance leakage, thereby improving the volumetric efficiency of the unit.

The leakage amount under different gap thicknesses is shown in Figure 6. When the inlet and outlet boundaries are constant, the gap thickness of the upper crown decreases, and the flow passage between the upper crown and the top cover expands. In addition, the flow through the gap increases accordingly, and the increase in the flow causes the pressure value inside the gap to decrease, thereby causing the water thrust value to decrease.

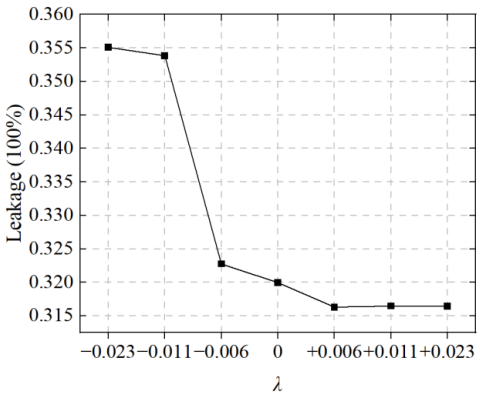

Figure 6. Leakage at different gap thicknesses.

3.4. Flow Field Analysis

3.4.1. Pressure Distribution at Different Gap Thicknesses

Different values of the crown seal gap of the runner have a disturbing effect on the flow field of the crown seal gap of the Francis turbine. It is necessary to carry out numerical simulation calculations of the whole channel of the prototype turbine and to then analyze the pressure field and velocity field. Because the flows in the upper and lower labyrinth rings basically do not affect each other, the change in the thickness of the upper coronal space mainly affects the flow in the upper coronal space.

It can be seen from the pressure calculation results that the pressure distribution under different gaps is basically the same. Only the labyrinth ring changes significantly, and the pressure value of the inlet and outlet changes with the gap. As shown in Figure 7, the pressure gradient distribution in the gap flow channel is relatively uniform. The maximum pressure is distributed at the inlet of the crown gap, and the minimum pressure is at the outlet. From the inlet to the outlet of the gap, the pressure decreases continuously along the flow direction, and the pressure energy of the liquid is converted into kinetic energy, which also proves the effectiveness of the labyrinth seal on the decompression of the liquid. The pressure near the pressure equalizing tube is the smallest, which also proves that the pressure equalizing tube has a depressurizing effect.

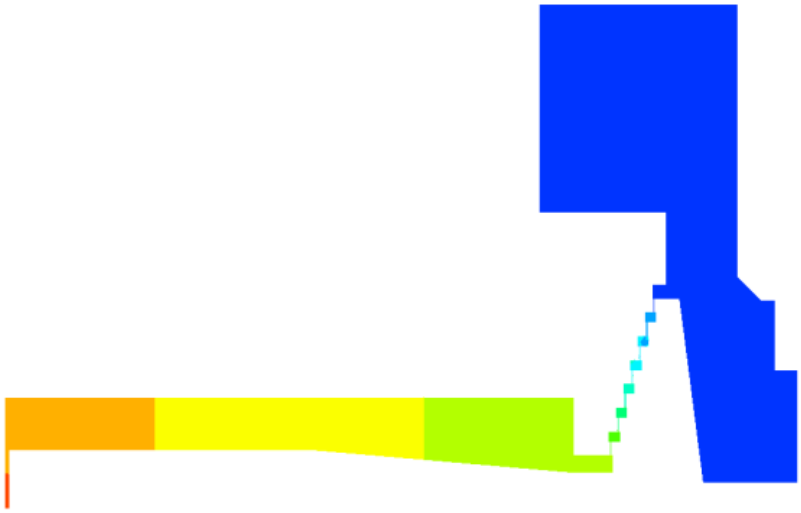

Figure 7. Pressure distribution of initial thickness.

As shown in Figure 7, when the thickness of the coronal gap is reduced, the pressure in the square cavity and narrow gap of the second-stage labyrinth ring near the exit of the gap changes. When λ decreases by 0.006 and 0.011, the pressure tends to be uniform, and when it decreases to 0.023, the pressure distribution is consistent with the original thickness. When the thickness of the coronal gap increases, the pressures in the square cavity and narrow gap of the first-level and second-level labyrinth rings near the exit of the gap decrease. When λ increases to 0.011 and 0.023, the pressure in the central area of the square cavity of the first-level labyrinth ring near the gap exit and the narrow gap connected to the pressure equalizing tube decreases significantly.

The pressure difference Δp between the inlet and outlet of the upper crown gap is shown in Figure 8. The pressure difference is larger when the thickness of the upper crown gap is smaller. The pressure difference is the largest when the thickness increases by 0.011, and the pressure difference is the smallest when the thickness is reduced by 0.011.

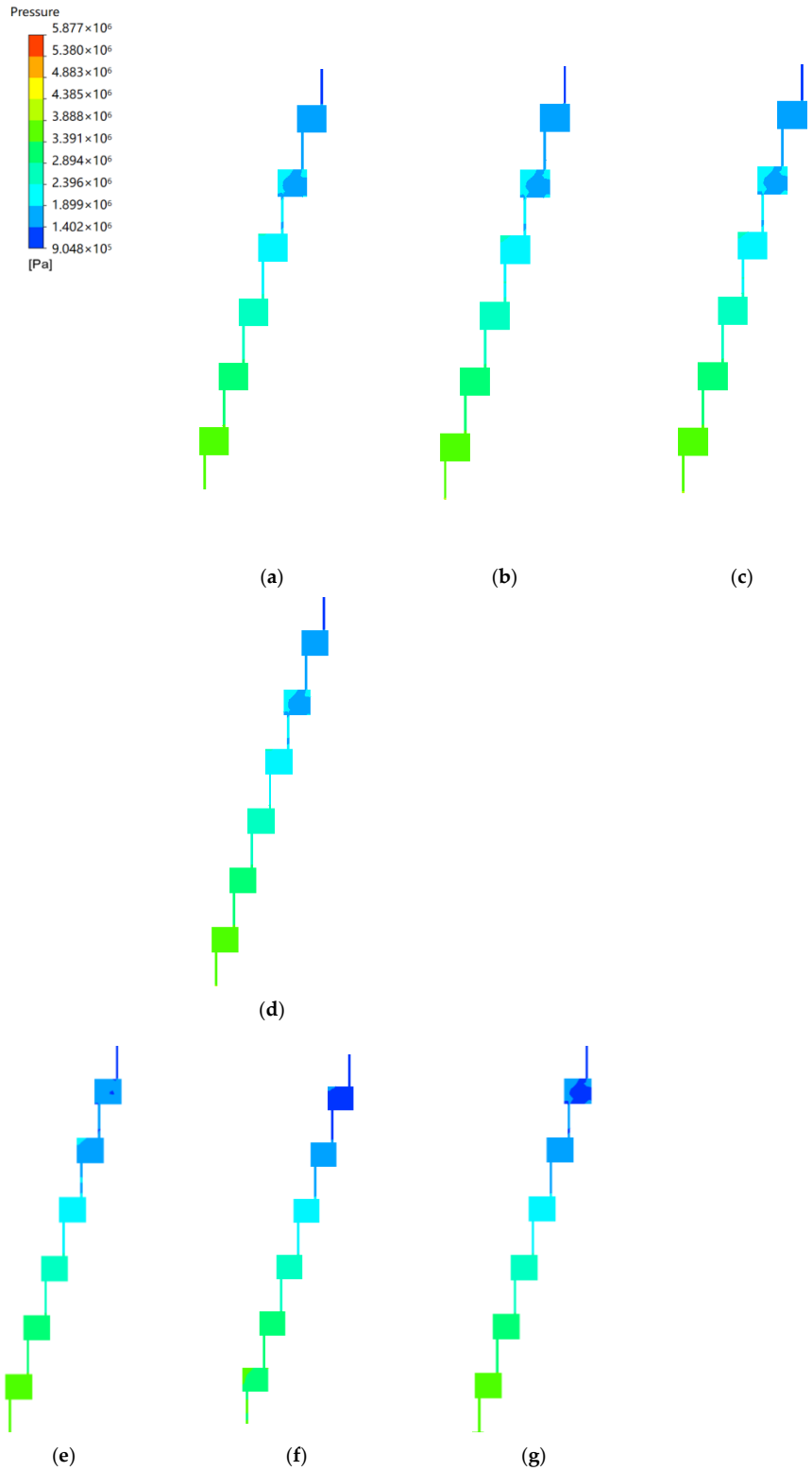

Figure 8. Pressure distribution of the labyrinth ring under different gap thicknesses: (**a**) Pressure distribution when $\lambda = -0.023$; (**b**) Pressure distribution when $\lambda = -0.011$; (**c**) Pressure distribution when $\lambda = -0.006$; (**d**) Pressure distribution when $\lambda = 0$; (**e**) Pressure distribution when $\lambda = +0.006$; (**f**) Pressure distribution when $\lambda = +0.011$; (**g**) Pressure distribution when $\lambda = +0.023$.

3.4.2. Velocity Distribution at Different Gap Thicknesses

For the design of the main stream flow parts of the turbine, the principle is to minimize the hydraulic loss of the flow parts, and for the design of the labyrinth ring, it is necessary to increase the energy loss in the gap of the labyrinth ring as much as possible to reduce the flow loss and power loss, thereby increasing the flow efficiency and power efficiency. As shown in Figure 9, the speed from the gap inlet to the outlet is a process of decreasing speed. The flow velocity at the gap inlet is relatively high, and the streamlines (noted as arrows) are relatively smooth. When the water flow passes through the labyrinth gap, it passes through many right-angle bends, the water flow resistance increases, the flow velocity decreases, and the hydraulic loss increases. Dispersion does not restore the pressure energy, and the energy loss of the liquid increases further. Moreover, with the increase in the gap, the vortex streamlines at the junction of the gap outlet of the upper crown and the flat pressure tube become denser, and the speed increases.

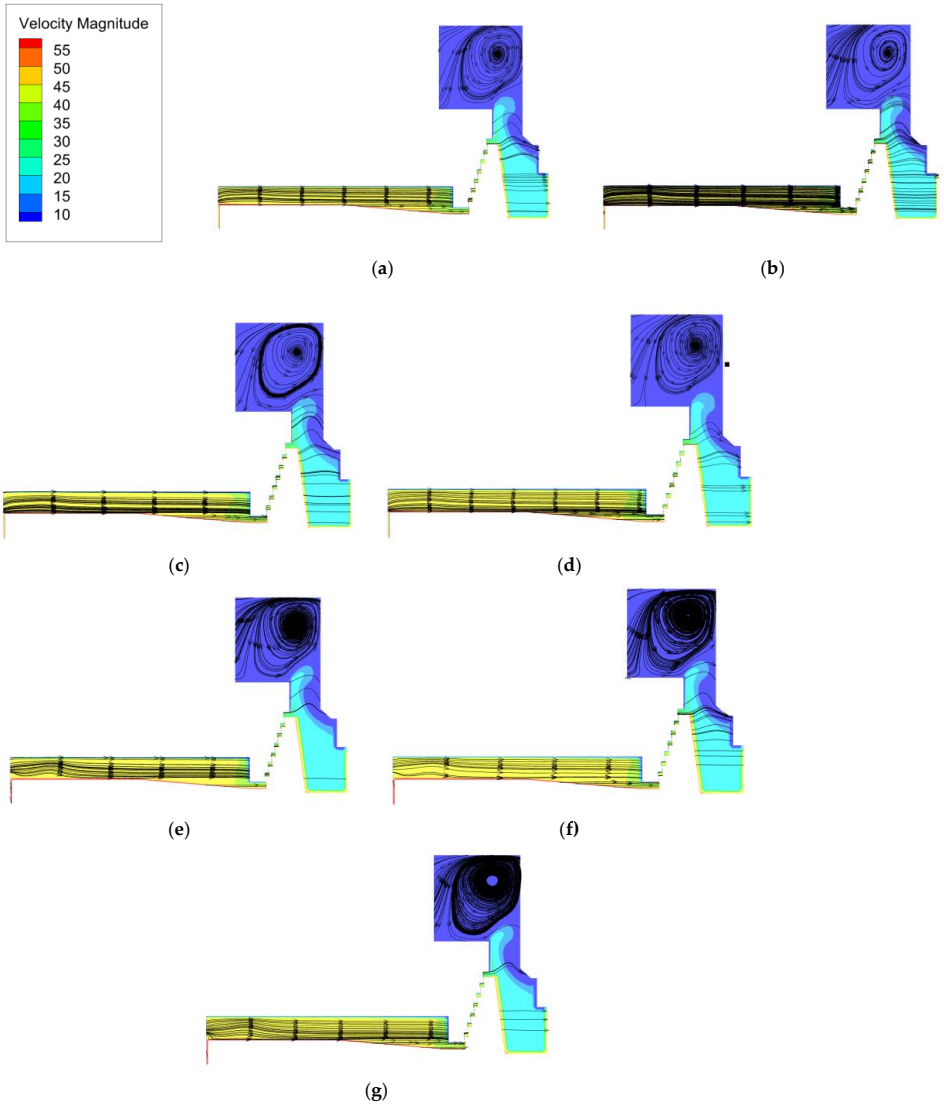

Figure 9. Velocity and streamline distribution of the labyrinth ring under different gap thicknesses. (**a**) Velocity and streamline distribution when $\lambda = -0.023$; (**b**) Velocity and streamline distribution when $\lambda = -0.011$; (**c**) Velocity and streamline distribution when $\lambda = -0.006$; (**d**) Velocity and streamline distribution when $\lambda = 0$; (**e**) Velocity and streamline distribution when $\lambda = +0.006$; (**f**) Velocity and streamline distribution when $\lambda = +0.011$; (**g**) Velocity and streamline distribution when $\lambda = +0.023$.

3.5. Monitoring Point Pressure under Different Gaps

The pressure pulsation of the pump turbine is one of the causes of hydraulic mechanical vibrations, especially in large-scale units, due to the large size and low stiffness of the unit. In addition, the instability of the water flow can easily cause unit vibration, and in severe cases, it can cause fatigue damage to the unit components. According to the locations of the pressure pulsation measuring points of the unit, pressure pulsation monitoring points are set up at seven locations, including the lower part of the fixed guide vane, the upper part of the vaneless area, the entrance of the upper crown, the front of the upper crown labyrinth ring, the back of the upper crown labyrinth ring, the entrance of the lower ring and the front of the lower ring labyrinth ring, as shown in Figure 10.

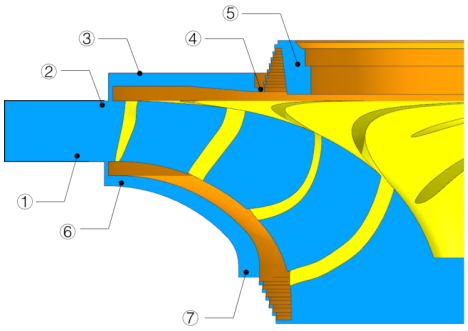

Figure 10. Schematic diagram of 7 monitoring points (①: Lower part of guide vanes; ②: Upper part of vaneless zone; ③: Crown inlet; ④: Crown labyrinth ring front; ⑤: Crown labyrinth ring rear; ⑥: Band inlet; ⑦: Band labyrinth ring front).

C_p is used to analyze the pressure of the pump turbine at different monitoring points.

$$C_p = \frac{P}{\rho g H_r} \tag{11}$$

Among them, P is the pressure measured at the monitoring point, and H_r is the rated water head value of the pump turbine under the turbine working condition.

The time domain diagram shown in Figure 11 shows that the pressure values of the pressure measuring points of each flow-passing component fluctuate relative to a certain reference value. Reducing the thickness of the upper crown gap has a weak effect on the pressure of the monitoring point, and increasing the thickness of the upper crown gap has a more obvious impact on the pressure at the entrance of the upper crown, in front of the labyrinth ring of the upper crown and in front of the labyrinth ring of the lower ring, which can reduce the pressure at the entrance of the upper crown and in front of the labyrinth ring of the upper crown. However, it increases the pressure in front of the labyrinth ring of the lower ring.

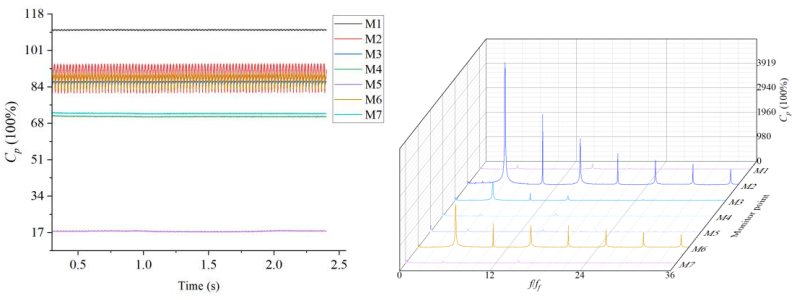

(**a**)

Figure 11. *Cont.*

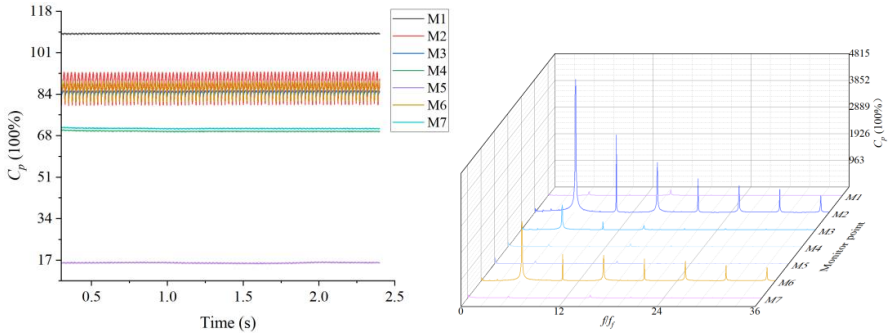

(**b**)

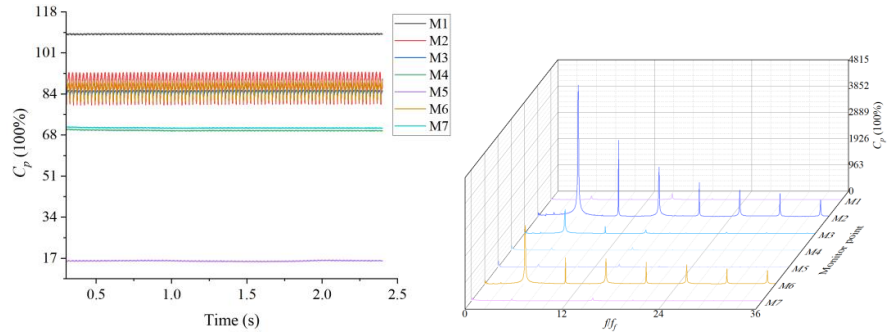

(**c**)

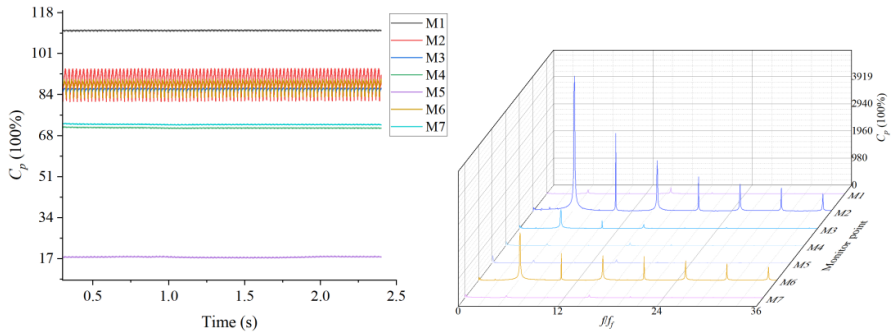

(**d**)

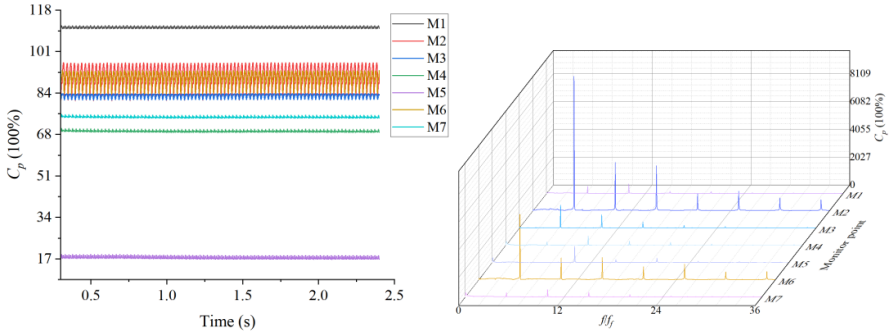

(**e**)

Figure 11. *Cont.*

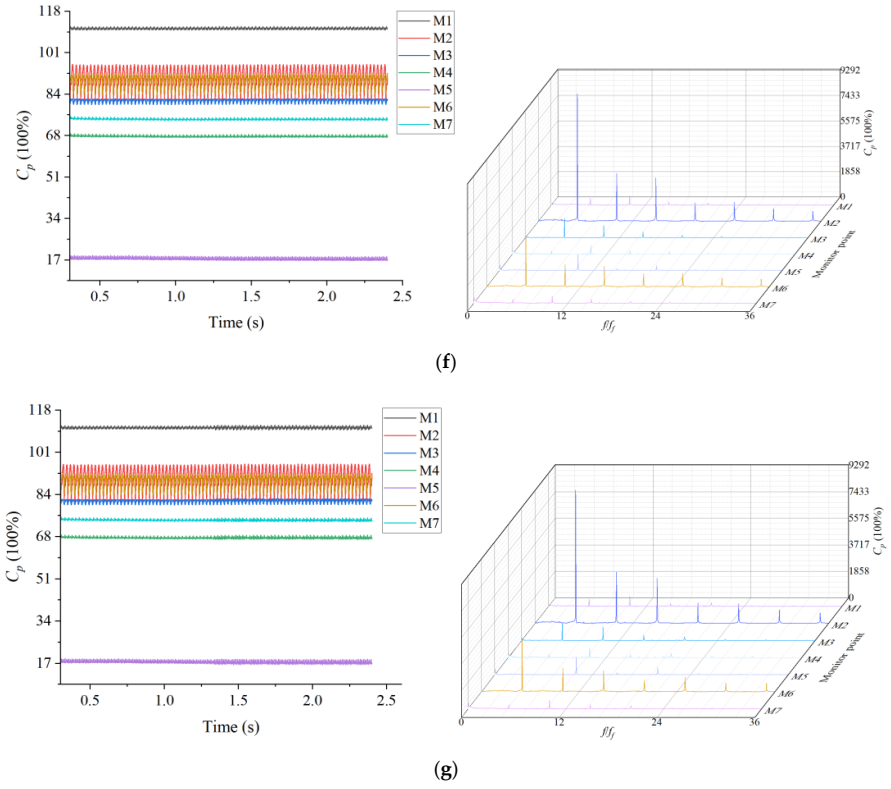

Figure 11. Monitor point pressure under different gap thicknesses: (**a**) Monitor point pressure when $\lambda = -0.023$; (**b**) Monitor point pressure when $\lambda = -0.011$; (**c**) Monitor point pressure when $\lambda = -0.006$; (**d**) Monitor point pressure when $\lambda = 0$; (**e**) Monitor point pressure when $\lambda = +0.006$; (**f**) Monitor point pressure when $\lambda = +0.011$; (**g**) Monitor point pressure when $\lambda = +0.023$.

According to the frequency spectrum, the lower part of the fixed guide vane is far away from the runner, and the water flow at the outlet of the guide vane is relatively smooth under rated conditions. Therefore, the pressure pulsation at the lower part of the fixed guide vane is relatively small. Because the streamlines in front of the upper crown labyrinth ring, behind the upper crown labyrinth ring and in front of the lower labyrinth ring are relatively smooth and the flow state is stable, the pressure change is not obvious. Because the upper part of the bladeless area, the inlet of the upper crown and the inlet of the lower ring are relatively close to the runner, the interference of the rotating parts is the strongest. Therefore, the pressure pulsation of these three parts is more obvious. The frequency components of the three monitoring points are basically the same under different gap thicknesses. They are the passing frequency of the runner blade and its harmonic frequency. The main frequency of the pressure pulsation is 5 times the rotation frequency, and the secondary frequency is 10 times the rotation frequency. Moreover, under the working conditions of the turbine, the high-speed water flow quickly enters the runner after passing through the guide vanes and impacts the working surface of the blade, which causes RSI between the guide vanes and the runner, resulting in severe vibration and the largest pressure pulsation in the bladeless area between the guide vanes and the runner. Therefore, the high-frequency components are mainly concentrated in the bladeless area. The collision between the water flow in the bladeless area and the blades is also one of the important hydraulic factors for the vibration of the turbine under the working conditions of the turbine.

The pressure fluctuations in the vaneless area, the entrance of the upper crown and the entrance of the lower ring are obvious, corresponding to the monitoring points M2, M3

and M4, respectively. The relationship between the peak value of the pressure fluctuation and the water head is shown in Equation (12).

$$R_P = \frac{\Delta P}{\rho g H} \tag{12}$$

Among them, P is the pressure of the measuring point, ρ is the density of water (1000 kg/m ^{3}), and g is the acceleration of gravity (9.8 m/s ^{2}).

Figure 12 shows the relative pressure fluctuations of the three monitoring points. When the gap thickness of the upper canopy is reduced, the relative pressure fluctuations of the vaneless area are not greatly affected, but the R_p values at the entrance of the upper canopy and the entrance of the lower ring increase. When the thickness of the gap is reduced to 0.023, the relative pressure fluctuations are almost the same as those corresponding to the original thickness. The relative pressure fluctuations in the vaneless area, upper crown entrance and lower ring entrance increase as the upper crown gap thickness increases, and the relative pressure fluctuation range is the largest when the upper crown gap thickness increases by 0.006.

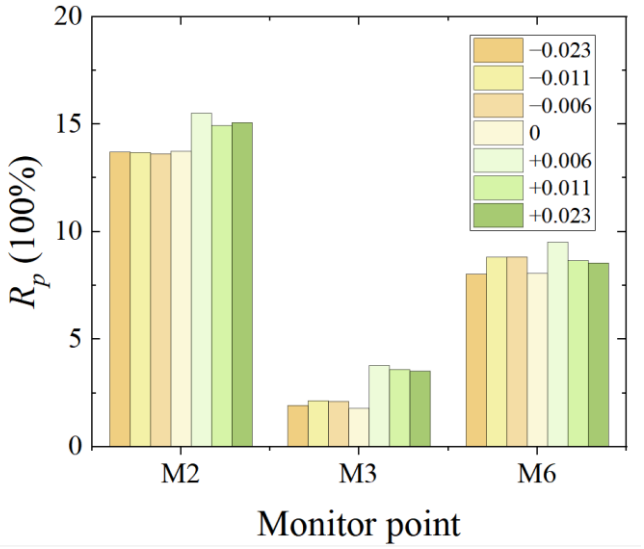

Figure 12. Relative pressure fluctuation amplitude of monitor points.

3.6. Axial Force at Different Gap Thicknesses

If the axial force is upward, it is easy to lift the machine, and if the axial force is downward, it increases the load and frictional power of the thrust bearing. That is to say, the design requirements for the thrust bearing are relatively high, and if the axial water thrust of the pump turbine is vertically downward and the value is large, especially in the case of strong pulsation of the unit, the water thrust has a dual effect on the self-weight of the unit, which easily leads to friction of the thrust bearing and excessive deformation of the frame.

The unsteady calculation of the three-dimensional full flow channel is performed by changing the thickness of the upper crown gap. The rotation frequency of the wheel is shown in Equation (13).

$$f_f = \frac{n}{60} \tag{13}$$

Among them, n is the speed of the runner, 500 r/min, and the rotation frequency is 8.33 Hz.

As shown in Figure 13, taking the vertical downward direction as positive, the axial water thrust on the upper crown is positive. When the thickness of the crown gap is reduced, the axial water thrust on the crown also decreases with little fluctuation. However, when

the thickness of the crown gap is reduced, the axial water thrust on the crown increases. By increasing the thickness of the crown gap, the main frequency of the axial water thrust on the crown is 10 f_f, and the secondary frequency is 15 f_f.

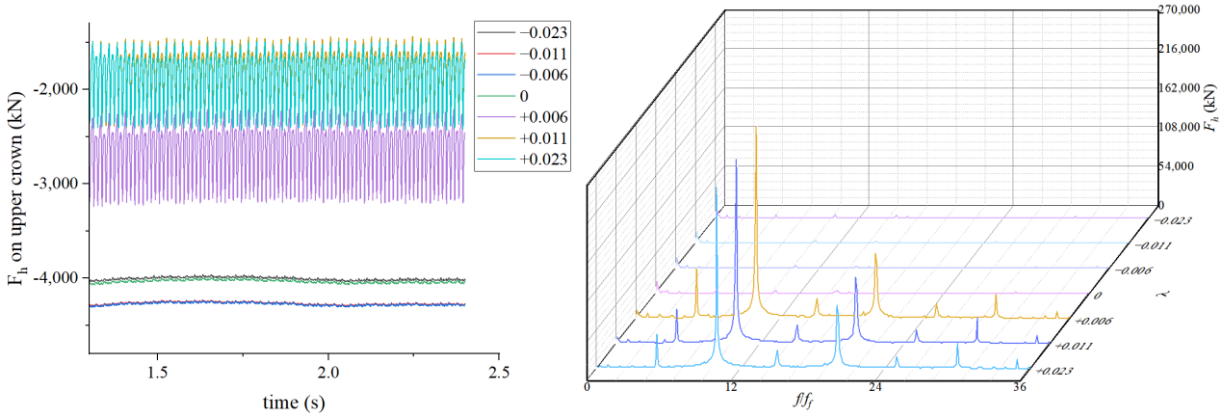

Figure 13. Time domain and frequency domain diagrams of axial hydraulic thrust on the upper crown.

As shown in Figure 14, taking the vertical upward direction as positive, the axial water thrust on the lower ring is positive. When the gap thickness λ of the upper crown is reduced by 0.006 and 0.011, the axial water thrust of the lower ring increases, and the axial force value is almost the same. When λ is reduced by 0.023, the axial water thrust of the lower ring has almost no change compared with the initial thickness. The axial water thrust on the lower ring also increases when λ is increased, and the axial water thrust on the lower ring is larger when the value is increased by 0.006 compared to increases of 0.011 and 0.023. By increasing the gap thickness of the upper crown, the main frequency of the axial water thrust on the lower ring is 10 f_f, and the secondary frequency is 15 f_f.

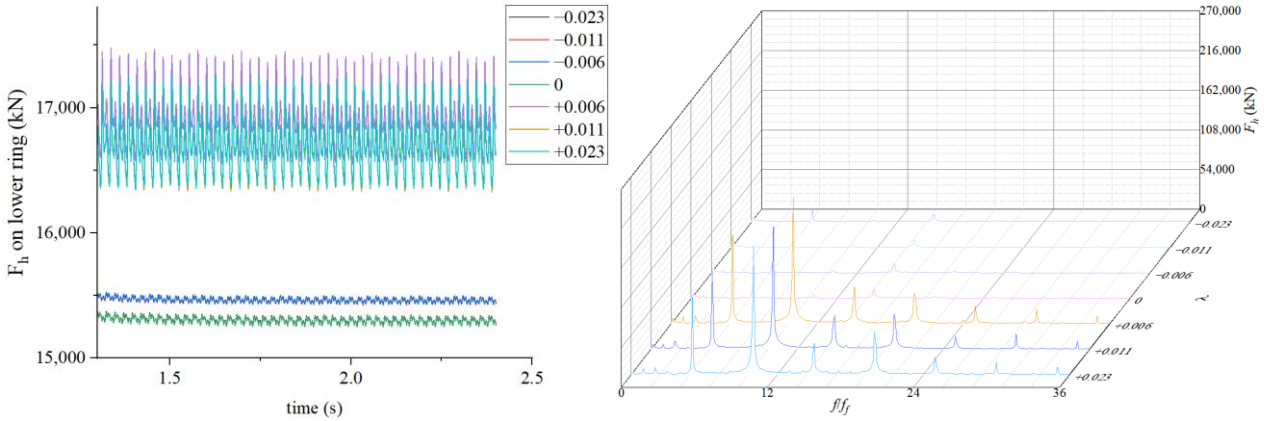

Figure 14. Time domain and frequency domain diagrams of axial water thrust on the lower ring.

The axial water thrust on the suction surface and pressure surface of the blade is shown in Figure 15, and the fluctuation of the axial water thrust on the blade is the largest when the increase is 0.023. Reducing the crown gap thickness has little effect on the axial water thrust of the blade. By increasing the crown gap thickness, the primary frequency of the axial water thrust on the blade is 10 f_f, and the secondary frequency is 15 f_f.

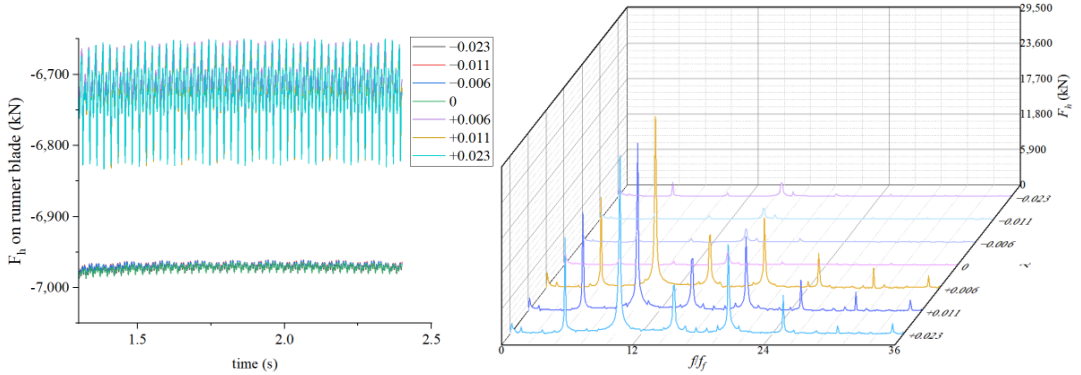

Figure 15. Time domain and frequency domain diagrams of axial water thrust on the runner blade.

The resultant force of the axial water thrust on the runner is shown in Figure 16. When the thickness of the upper crown gap is reduced, the resultant force of the axial water thrust decreases to about 77 kN, but the value of the resultant force increases slightly when it decreases to 0.023. When the thickness of the upper crown gap is increased, the axial water thrust increases greatly, and the resultant force increases the most when it increases by 0.011, which is about 3828 kN. By increasing the crown gap thickness, the main frequency of the resultant axial water thrust on the runner is 10 f_f, and the secondary frequency is 15 f_f.

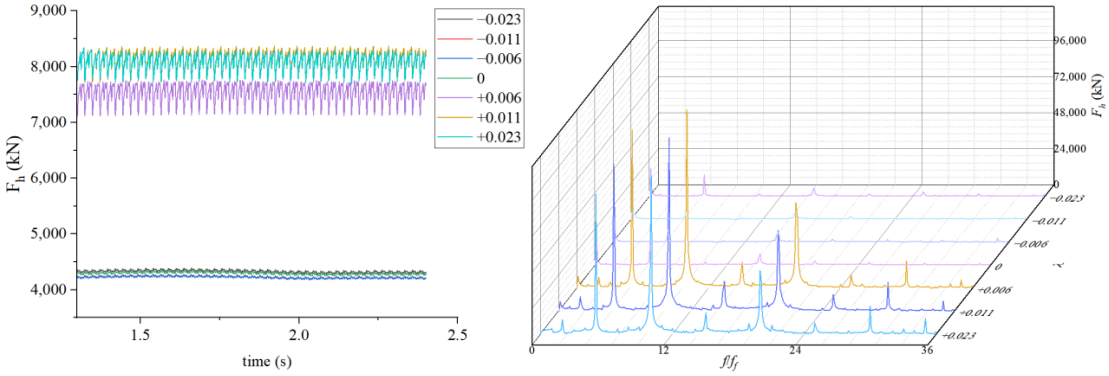

Figure 16. Time domain and frequency domain diagram of axial water thrust force.

The results show that increasing or decreasing the thickness of the upper crown gap can effectively change the axial water thrust and the resultant force of the axial water thrust on the upper crown and lower ring. However, the axial water thrust on the blade is only sensitive to increases in the thickness of the upper crown gap, and reducing the thickness hardly changes the axial water thrust on the blade. Increasing the thickness of the upper crown gap has a greater impact on the resultant axial hydraulic thrust compared to reducing the thickness of the upper crown gap. The thickness of the upper crown gap only increases by 0.006, and the average value of the resultant axial hydraulic thrust increases by about 3240 kN compared with the original gap thickness. Decreasing the thickness of the upper crown gap can reduce the axial water thrust. When the gap thickness λ of the upper crown is increased, the value of the axial water thrust and the resultant force of the axial water thrust on the upper crown, the lower ring and the blade increases greatly, and the pulsation frequency also increases significantly. The water thrust changes periodically with time, with a main frequency of 10 f_f and a secondary frequency of 15 f_f. When the gap thickness of the upper crown is reduced, the overall change in the axial water thrust and the resultant force of the axial water thrust on the upper crown, lower ring and blade is relatively stable. The effect of reducing λ by 0.006 and 0.011 is similar, but reducing it by 0.023 slightly increases the resultant force of the axial water thrust.

4. Conclusions

In this paper, a reversible pump turbine unit with different crown clearances was studied by means of CFD numerical simulations. The pressure distribution, energy characteristics and axial hydraulic force were obtained and analyzed. It was found that the crown clearance has a significant influence on the flow pattern and axial force of the runner. The main conclusions are displayed below.

(1) As the thickness of the crown gap decreases, the flow channel between the crown and the top cover expands, and the leakage through the crown gap increases. The change in the thickness of the crown gap mainly affects the internal flow field of the crown gap. The pressure and velocity distribution of the crown under different crown gap thicknesses are basically the same, and the area with a large change is at the seal of the labyrinth ring. The seal of the labyrinth ring and the pressure equalizing tube can reduce the pressure of the upper crown gap. The pressure of the labyrinth ring does not change significantly when the gap thickness is reduced. Increasing the gap thickness reduces the pressure of the square cavity and narrow gap of the first and second labyrinth rings near the exit of the gap. The pressure equalizing tube has a great influence on the flow rate through the gap, and the upper crown gap near the pressure equalizing tube generates vortices, resulting in energy loss.

(2) The pressure value of the monitoring point is not sensitive to decreases in the upper crown clearance thickness, in front of the upper labyrinth ring and in front of the lower labyrinth ring. Because the upper part of the vaneless area, the inlet of the upper crown and the inlet of the lower ring are relatively close to the runner, the interference of the rotating parts is the strongest, so the pressure pulsation changes obviously. The main frequency of the pressure pulsation is 5 times the rotation frequency, and the secondary frequency is 10 times the rotation frequency. Because of the rotor–stator interaction between the guide vanes and the runner, the high-frequency components of the pressure pulsation are mainly concentrated in the vaneless area.

(3) Changing the thickness of the upper crown gap can effectively change the axial water thrust and the resultant force of the upper crown and lower ring, but the axial water thrust of the blade is only sensitive to increases in the upper crown gap thickness. The overall change in the axial hydraulic thrust is relatively stable when the thickness of the upper crown gap is reduced. Increasing the gap thickness of the upper crown has a greater effect on the resultant axial hydraulic thrust compared to decreasing the gap thickness of the upper crown. Increasing the gap thickness increases the value of the axial hydraulic thrust and the resultant axial hydraulic thrust on the upper crown, lower ring and blade, and the pulsation frequency also increases significantly.

Author Contributions: Conceptualization, L.L. and D.Y.; methodology, D.Y. and X.L.; software, D.Y. and W.Z.; validation, X.L. and W.Z.; formal analysis, Y.W.; investigation, L.L.; resources, Z.W.; data curation, D.Y.; writing—original draft preparation, J.P.; writing—review and editing, D.Y.; visualization, L.L.; supervision, X.L.; project administration, Y.W.; writing-original draft preparation, J.P.; funding acquisition, W.Z. All authors have read and agreed to the published version of the manuscript.

Funding: This work was funded by the China Postdoctoral Science Foundation (Grant No. 2022M711768) and was supported by the Joint Open Research Fund Program of State Key Laboratory of Hydroscience and Engineering and the Tsinghua–Ningxia Yinchuan Joint Institute of Internet of Waters on Digital Water Governance (sklhse-2022-Iow13).

Data Availability Statement: The data is unavailable due to privacy.

Acknowledgments: The authors express sincere gratitude for the financial assistance of the following project: the pump turbine shaft coupling performance review calculation project of Henan Luoning Pump-storage Power Co., Ltd.

Conflicts of Interest: The authors declare no conflict of interest.

References

1. Ferreira, H.L.; Garde, R.; Fulli, G.; Kling, W.; Lopes, J.P. Characterisation of electrical energy storage technologies. *Energy* **2013**, *53*, 288–298. [CrossRef]
2. Hebner, R.; Beno, J.; Walls, A. Flywheel batteries come around again. *IEEE Spectr.* **2002**, *39*, 46–51. [CrossRef]
3. Rehman, S.; Al-Hadhrami, L.M.; Alam, M.M. Pumped hydro energy storage system: A technological review. *Renew. Sustain. Energy Rev.* **2015**, *44*, 586–598. [CrossRef]
4. Ackermann, T. *Wind Power in Power Systems*, 2nd ed.; Wiley: West Sussex, UK, 2012.
5. *Medium and Long Term Development Plan for Pumped Storage (2021–2035)*; National Energy Administration of China: Beijing, China, 2021.
6. Mei, Z. *Pumped Storage Technology*; Tsinghua University Press: Beijing, China, 1999.
7. Bouderlique, R.M.; Guibault, F.O.; Garon, A.; Vu, T. A Computational Model for Hydraulic Labyrinth Seals. In Proceedings of the ASME 2010 3rd Joint US-European Fluids Engineering Summer Meeting Collocated with 8th International Conference on Nanochannels, Microchannels, and Minichannels, ASME 2010 3rd Joint US-European Fluids Engineering Summer Meeting, Symposia—Parts A, B, and C, Montreal, QC, Canada, 1–5 August 2010; Volume 1, pp. 23–31.
8. Kim, S.J.; Choi, Y.S.; Cho, Y.; Choi, J.W.; Hyun, J.J.; Joo, W.G.; Kim, J.H. Effect of the leakage flow in runner on flow characteristics of a Francis turbine model. *IOP Conf. Ser. Earth Environ. Sci.* **2021**, *774*, 012087. [CrossRef]
9. Fu, X.; Li, D.; Wang, H.; Zhang, G.; Li, Z.; Wei, X. Influence of the clearance flow on the load rejection process in a pump-turbine. *Renew. Energy* **2018**, *127*, 310–321. [CrossRef]
10. Hou, X.; Liu, H.; Cheng, Y.; Liu, K.; Liu, D.; Chen, H. Clearance flow patterns and pressure distribution of a pump-turbine: Measurement and simulation of a rotating disk flow. *Front. Energy Res.* **2022**, *10*, 910834. [CrossRef]
11. Liu, Y.; Liu, C.; Zhang, Y.; Huang, X.; Guo, T.; Zhou, L.; Wang, Z. Influence of Axial Installation Deviation on the Hydraulic Axial Force of the 1000 MW Francis Runner in the Rated Operating Condition. *Energies* **2023**, *16*, 1878. [CrossRef]
12. Zhou, L.; Shi, W.; Li, W.; Agarwal, R. Numerical and Experimental Study of Axial Force and Hydraulic Performance in a Deep-Well Centrifugal Pump With Different Impeller Rear Shroud Radius. *J. Fluids Eng.* **2013**, *135*, 104501. [CrossRef]
13. He, L.; Zhou, L.; Ahn, S.H.; Wang, Z.; Nakahara, Y.; Kurosawa, S. Evaluation of gap influence on the dynamic response behavior of pump-turbine runner. *Eng. Comput.* **2019**, *36*, 491–508. [CrossRef]
14. Wang, Z.; Zhu, B.; Wang, X.; Qin, D. Pressure Fluctuations in the S-Shaped Region of a Reversible Pump-Turbine. *Energies* **2017**, *10*, 96. [CrossRef]
15. Yang, S.S.; Liu, H.L.; Kong, F.Y.; Xia, B.; Tan, L.W. Effects of the Radial Gap Between Impeller Tips and Volute Tongue Influencing the Performance and Pressure Pulsations of Pump as Turbine. *J. Fluids Eng.* **2014**, *136*, 054501. [CrossRef]
16. Peng, G.; Hong, S.; Chang, H.; Fan, F.; Zhang, Y.; Peng, S.H. Numerical and Experimental Research on the Influence of Clearance Between Impeller and Cover on the Pump Performance. *Mechanika* **2022**, *28*, 67–72. [CrossRef]
17. Yonezawa, K.; Watamura, T. Experimental and Numerical Investigations of Erosion on Runner Seal of a Francis Turbine. In Proceedings of the 30th IAHR Symposium on Hydraulic Machinery and Systems (IAHR 2020), Lausanne, Switzerland, 21–26 March 2021.
18. Sonawat, A.; Choi, Y.S.; Kim, K.M.; Kim, J.H. Parametric study on the sensitivity and influence of axial and radial clearance on the performance of a positive displacement hydraulic turbine. *Energy* **2020**, *201*, 117587. [CrossRef]
19. Sato, K.; He, L. Numerical investigation into the effects of a radial gap on hydraulic turbine performance. *Proc. Inst. Mech. Eng. Part A-J. Power Energy* **2001**, *215*, 99–107. [CrossRef]
20. Shu, P.; Sun, T.; Yu, Q.; Li, G.; Yu, W.; Shi, Z. Numerical investigation of the effect of axial clearance on the last stage of marine turbine. *Ocean. Eng.* **2022**, *266*, 112711. [CrossRef]